EUROPEAN ORGANIZATION FOR NUCLEAR RESEARCH
CERN – ACCELERATORS AND TECHNOLOGY SECTOR

CERN-ATS-2010-027

Test of a Diamond Detector Using Unbunched Beam Halo Particles

Bernd Dehning, Ewald Effinger, CERN BE/BI
Heinz Pernegger, Daniel Dobos, CERN PH/ADE
Helmut Frais-Kölbl, Fachhochschule Wiener Neustadt, Austria
Erich Griesmayer (corresponding author), Cividec Instrumentation*

Abstract

A pCVD diamond detector has been evaluated as a beam loss monitor for future applications in the LHC accelerator. The test monitor was mounted in the SPS BA5 downstream of a LHC collimator during the LHC beam set-up. CVD diamond particle detectors are already in use in the CERN experiments ATLAS, CMS, LHCb and Alice. This is a proven technology with high radiation tolerance and very fast signal read-out. It can be used for single-particle detection, as well as for measuring particle cascades, for timing measurements on the nanosecond scale and for beam protection systems. Despite the read-out being made through 250 m of CK50 cable, the tests have shown a very good signal-to-noise ratio of 6.8, an excellent double-pulse resolution of less than 5 ns and a high dynamic range of 1:350 MIP particles. The efficiency of particle detection is practically 100% for charged particles.

Geneva, Switzerland
February, 2010

* Cividec Instrumentation GmbH, Bäckerstrasse 1, A-1010 Vienna, www.cividec.at

1 Introduction

CVD[**]-diamond particle detectors are already in operational use as beam conditions monitors in the CERN experiments ATLAS, CMS, LHCb and Alice. This is a proven technology with high radiation tolerance and fast signal read-out. The high dynamic range covers single-particle detection with a double-pulse resolution of 1 ns up to the resolution of particle cascades limited by the saturation of the electronics [1].

In the present tests, a specially-built diamond detector was placed downstream of a collimator in the SPS BA5 during the beam set-up for LHC to intercept particle showers from off-orbit protons. The high temporal resolution and the fast recovery time make it possible to detect the arrival of particles between the nominal bunch positions.

Descriptions are given of the detector, the measurement set-up and the measurement modes with a discussion of the performance and applications.

2 The Diamond Beam Monitor

The basic detector element is a 10 mm × 10 mm × 0.5 mm pCVD substrate with an active rectangular area of 8 mm × 8 mm, see Figure 1. Gold electrodes on the upper and lower surfaces collect the ionisation charge. The ceramics board is 44 mm × 34 mm. There are four holes for mounting the basic elements into a stack and two small holes for alignment. The LHC DBM consists of a stack of two modules. Some CVD diamond parameters are given in Table 1.

Mass number	12
Atomic number	6
Dielectric constant	5.7
Band gap	5.45 eV
Ionization energy	13 eV
Ionization linear density	36 e-h pairs/μm
Resistivity	$>10^{15}$ Ωcm
Radiation tolerance	$5x10^{15}$ protons/cm^2 (equals 1.25 MGy)

Table 1: Relevant pCVD diamond parameters.

[**] CVD=chemical vapour deposition and pCVD=polycrystalline chemical vapour deposition.

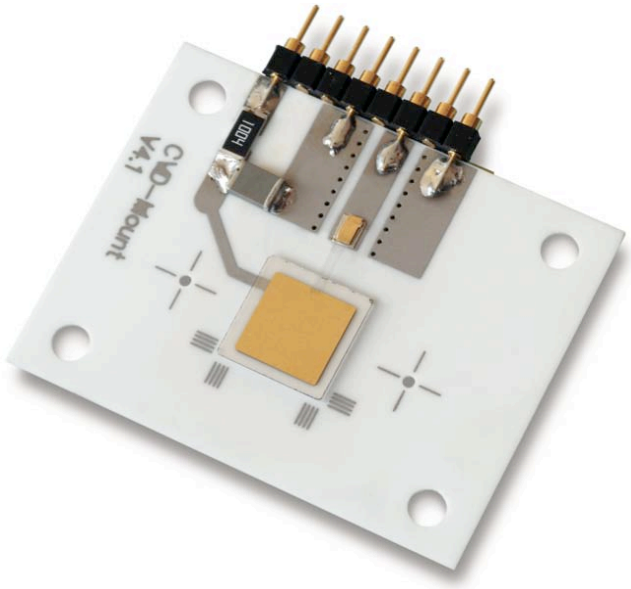

Figure 1: Basic CVD diamond detector element.

The CVD diamond particle detector functions as an ionisation chamber. Ionising particles that cross the detector stack liberate charges that are collected by applying a voltage of 500 V. The use of multiple layers improves the signal-to-noise ratio. The majority of particles entering the detector are not absorbed, but the confidence level that a particle is detected is practically 100%. A fast preamplifier and a high-quality signal cable complete the beam monitor.

2.1 Lifetime of the detector and its electronics

CVD diamond material is suitable for applications in very high-radiation environments such as the LHC. CVD diamond detector materials have been tested for their radiation tolerance [2].

2.1.1 Detector

With increasing irradiation, the detector response amplitude decreases exponentially (Figure 2). A decrease of 15% was observed at a fluence of 1×10^{15} p/cm^2, a decrease of 25% at an irradiation of 2.2×10^{15} protons/cm^2, 1/e at 12.5×10^{15} p/cm^2, and 75% at an irradiation fluence of 20×10^{15} p/cm^2 which corresponds to an irradiation dose of 5 MGy [3].

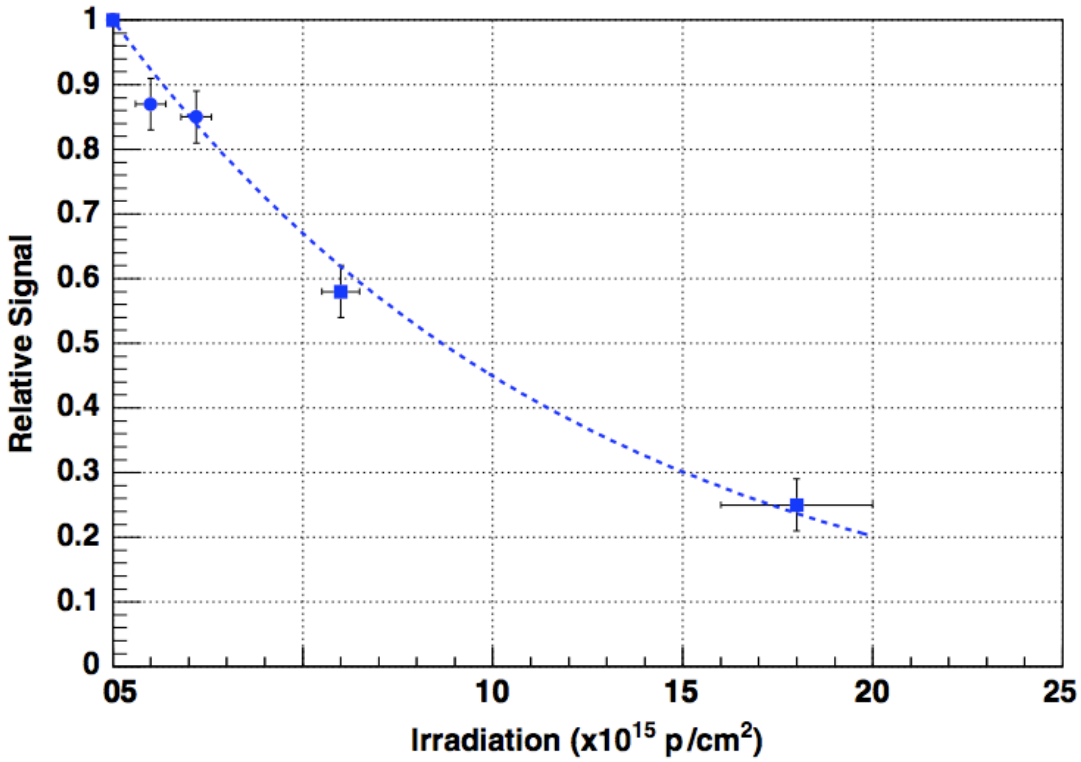

Figure 2: RD42 lifetime measurements of pCVD diamond detector material when irradiated with 24 GeV protons at the CERN PS [2].

2.1.2 Electronics

For the application at ATLAS BCM [4], CVD diamond detectors and preamplifiers were designed for an irradiation of 1×10^{15} protons/cm^2, which is the expected dose at LHC over a period of 10 years. Irradiation of preamplifiers was performed with protons, neutrons and photons. An amplification loss of 20% was observed at irradiation levels of 1×10^{15} protons/cm^2 (0.25 MGy).

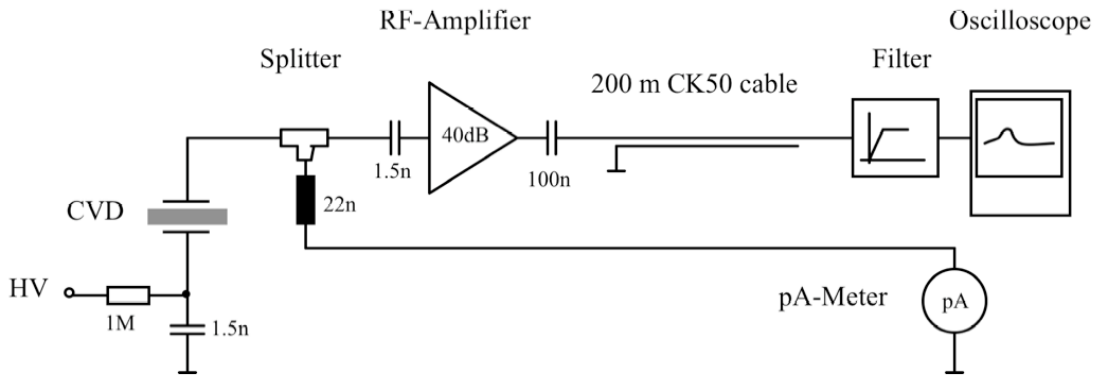

Figure 3: Schematic view of the overall monitor system.

3 Test set-up

The diamond detector was installed in SPS BA5, directly under the SPS beam vacuum chamber and about 2 m downstream of a LHC collimator, see Figure 4. Some 250 m of CK50 coaxial signal cable, HV and LV supply cables and monitoring cables linked the detector to the counting room.

Figure 4: The detector is installed in BA5 directly below the beam vacuum chamber and about 2 m downstream of the LHC collimator.

The schematic diagram in Figure 3 shows the overall monitor system set-up. The ionization charge from the detector appears as a current source on the high voltage side that is connected via a load resistor and capacitor to the ac-coupled pre-amplifier that has a 40 dB gain and 1 GHz bandwidth. The detector dark current is monitored via a RF splitter placed upstream of the coupling capacitor. A 250 m long CK50 cable connects the detector in SPS BA5 to the instrumentation in the counting room where a bandpass filter with 200 kHz low cut-off frequency and 200 MHz high cut-off frequency is used to reduce low-frequency and high-frequency noise. Data recording is done with a digital oscilloscope (LeCroy WaveRunner 104MXi-A, 1 GHz, 10 GS/s).

4 Detector characterization

Before operation in the SPS the detector was characterized concerning its signal response. The amplitude distribution and the SNR, the timing behaviour and the charge yield were measured.

4.1 Amplitude distribution

The most relevant figure for single-particle measurement is the signal-to-noise ratio, which is defined as the ratio of the peak amplitude of the detector signal to the rms baseline noise.

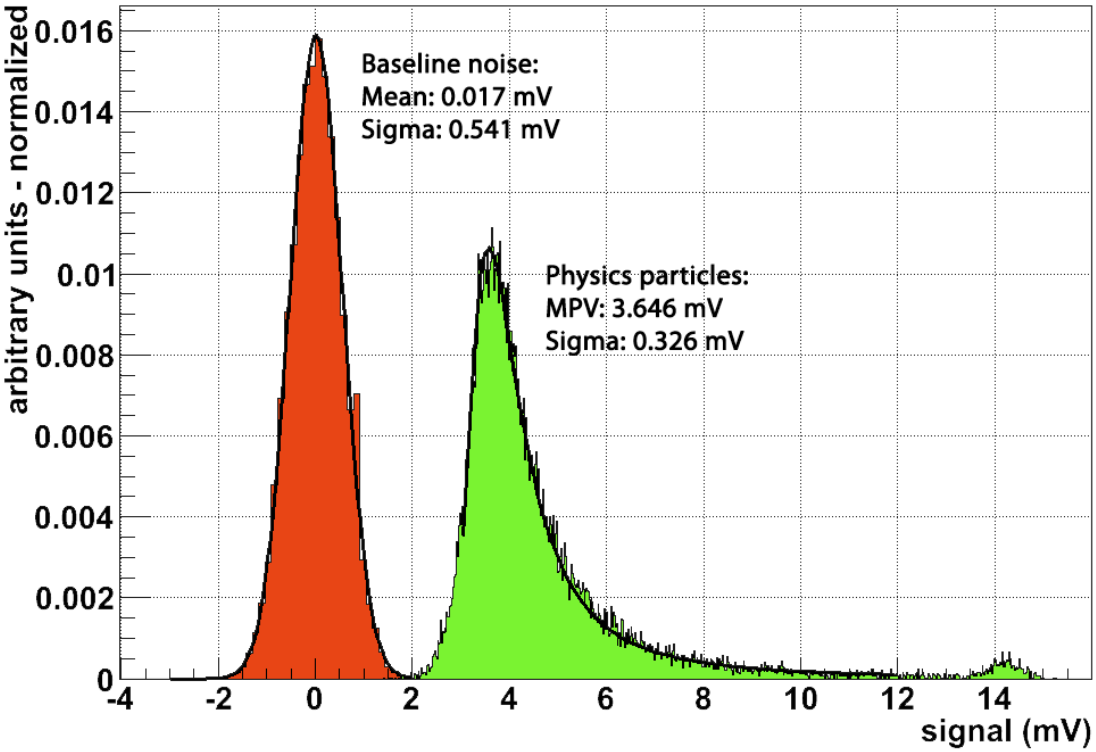

Figure 5: Gauss fit of the baseline noise distribution and Landau fit of physics events.

Figure 5 shows the Gaussian amplitude distribution of the baseline noise and the Landau amplitude distribution of physics particles measured in the SPS. The Landau distribution consists of events of many different particle types and energies. It is well separated from the noise distribution.

The Gauss fit of the baseline noise shows a sigma of 0.541 mV and the Landau fit of the physics events has a most probable value (MPV) of 3.646 mV. This results in a SNR of 6.8.

The preamplifier saturates at 1.3 V, which corresponds to a dynamic range from 1 MIP to 350 MIP particles and to a maximum detector current of 220 μA.

4.2 Timing behaviour

Figure 6 shows an average pulse, which was measured in the lab with a ^{90}Sr source using a 1 m long signal cable. The amplitude is 6.20 mV, the rise time 929 ps, the pulse width 1.528 ns and the fall time 1.406 ns.

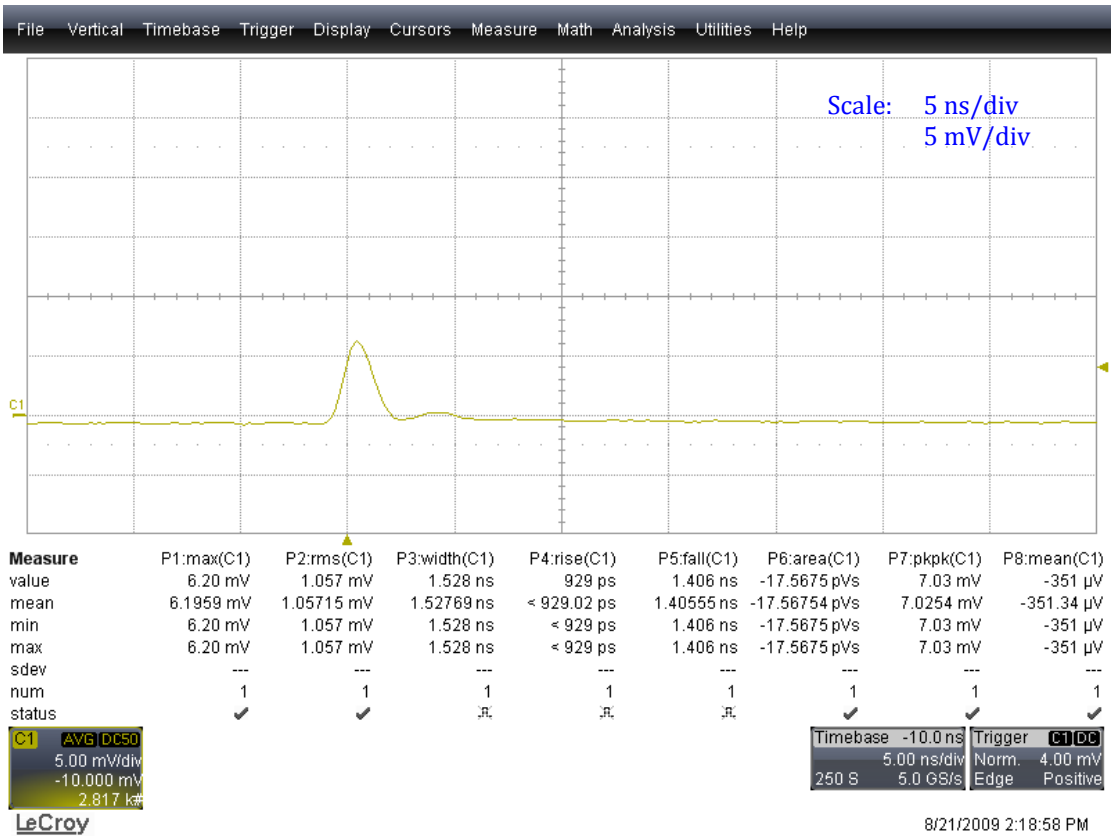

Figure 6: Average pulse measured in the lab using a ^{106}Sr source.

The timing of the detector in the SPS tunnel was evaluated using a ^{106}Ru source. Figure 7 shows the histograms of the amplitudes (yellow), rise time (pink), pulse width (blue), the pulse area (green) and a single pulse.

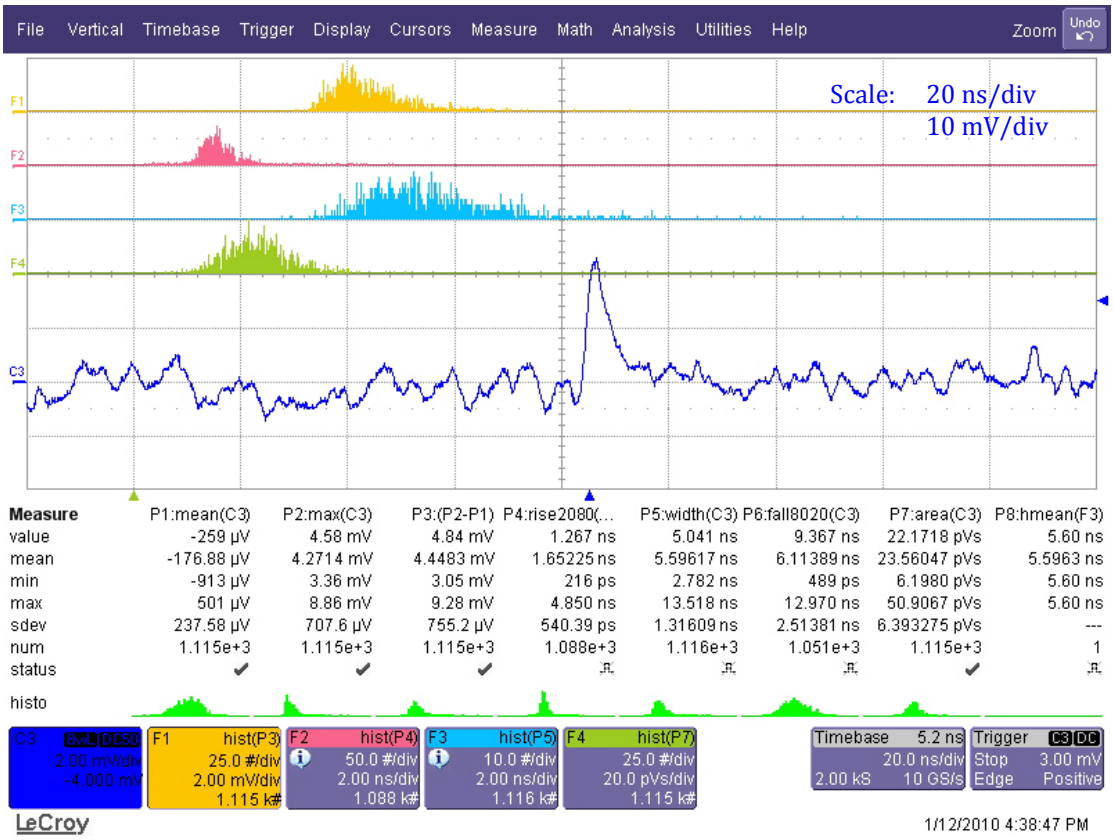

Figure 7: The histograms of the amplitudes (yellow), rise time (pink), pulse width (blue), the pulse area (green) and a single pulse.

The average rise time for MIP* particles is 1.652 ns, the average pulse width (defined as FWHM** of the signal) is 5.596 ns and the average fall time is 6.114 ns.

The degradation in timing is caused by dispersion in the 250 m long cable.

4.3 Charge yield

As shown in Figure 7 the average pulse area is 23.56 pVs. In the 50 Ω system, this corresponds to a charge of 3.93 fC deposited in the detector (considering the preamplifier gain of 120). This corresponds to 12'200 electron-hole pairs for two CVDs and to 6100 electron-hole pairs for a single CVD, respectively, which are generated per MIP in the detector.

* Minimum Ionising Particle
** Full Width at Half Maximum

5 Measurements

During the LHC set-up, the monitor system was operated under three distinct modes of SPS beam operation:

- ➔ Fixed-target physics beam,
- ➔ coasting beam,
- ➔ LHC beam.

All amplitude measurements used a baseline correction and a slew-rate trigger of >2 mV/ns.

There are five modes of detector operation:

- ➔ Single-particle mode,
- ➔ multi-particle mode,
- ➔ cascade mode,
- ➔ high intensity mode,
- ➔ background.

5.1 Single-particle mode

Figure 8 shows a single-particle pulse measured in the SPS with a ^{106}Ru source. The example shows an amplitude of 3.83 mV, a rise time of 1.327 ns, a pulse width of 4.583 ns and a fall time of 4.667 ns.

Figure 9 shows an average pulse of the detector measured with a ^{106}Ru source. The amplitude is 4.244 mV, the rise time 1.532 ns, the pulse width 4.981 ns and the fall time 5.327 ns.

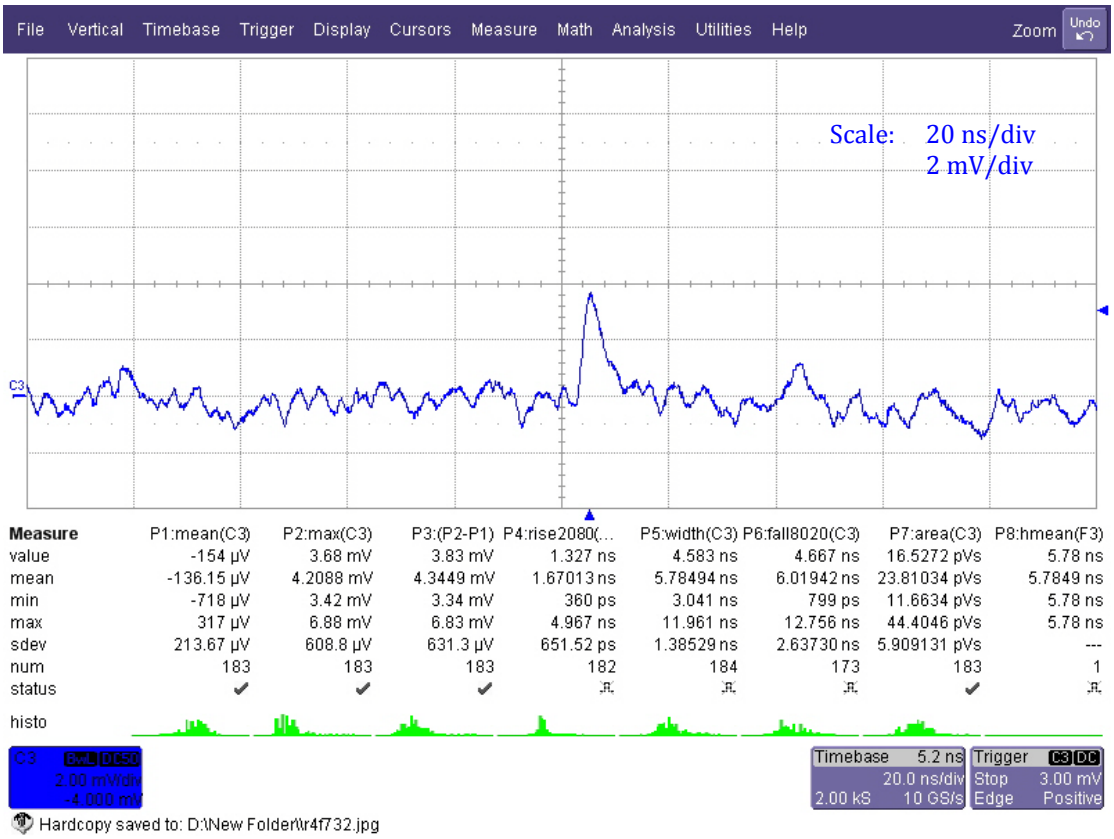

Figure 8: Single particle pulse measured in the SPS using a ^{106}Ru source.

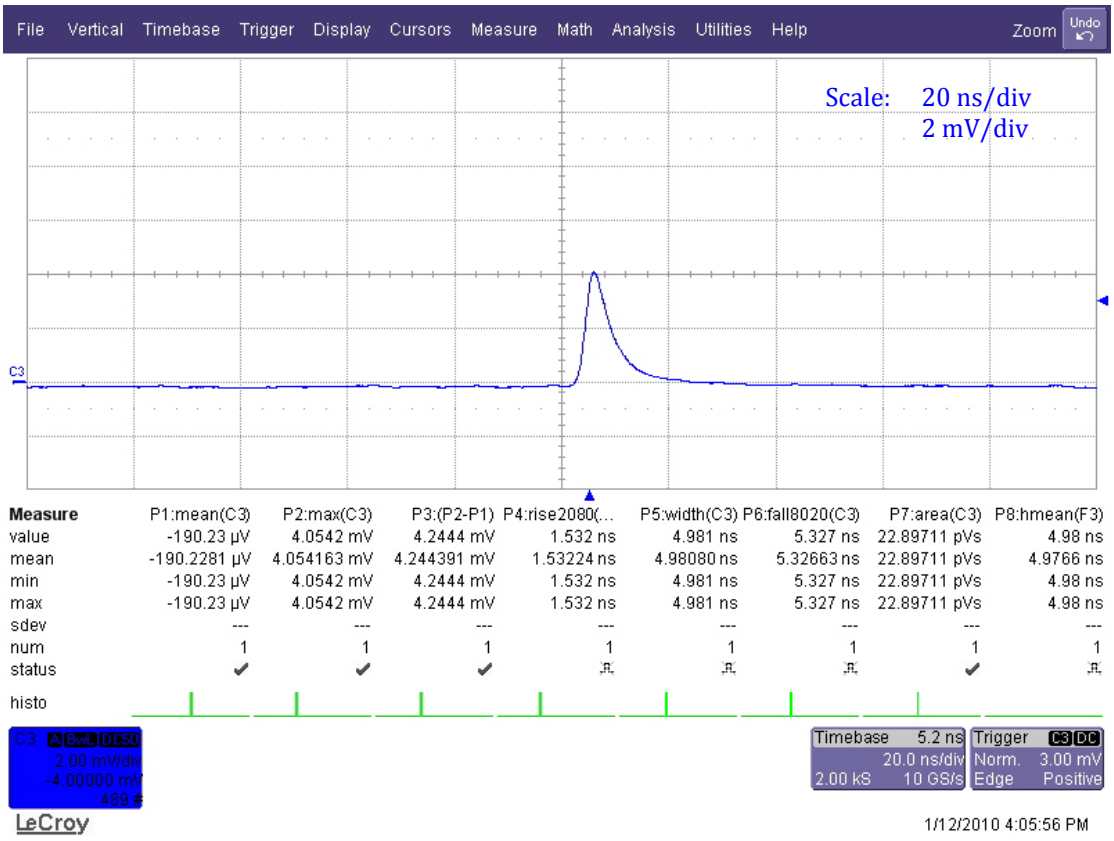

Figure 9: Average particle pulse measured in the SPS using a ^{106}Ru source.

5.2 Multi-particle mode

Figure 10 shows the persistence mode of several multi-particle events. The linear behaviour of the system is well demonstrated.

Figure 11 shows a multi-particle pulse with an amplitude of 103 mV and a FWHM of 3.9 ns.

The amplitude corresponds to 28 MIP particles hitting the detector simultaneously.

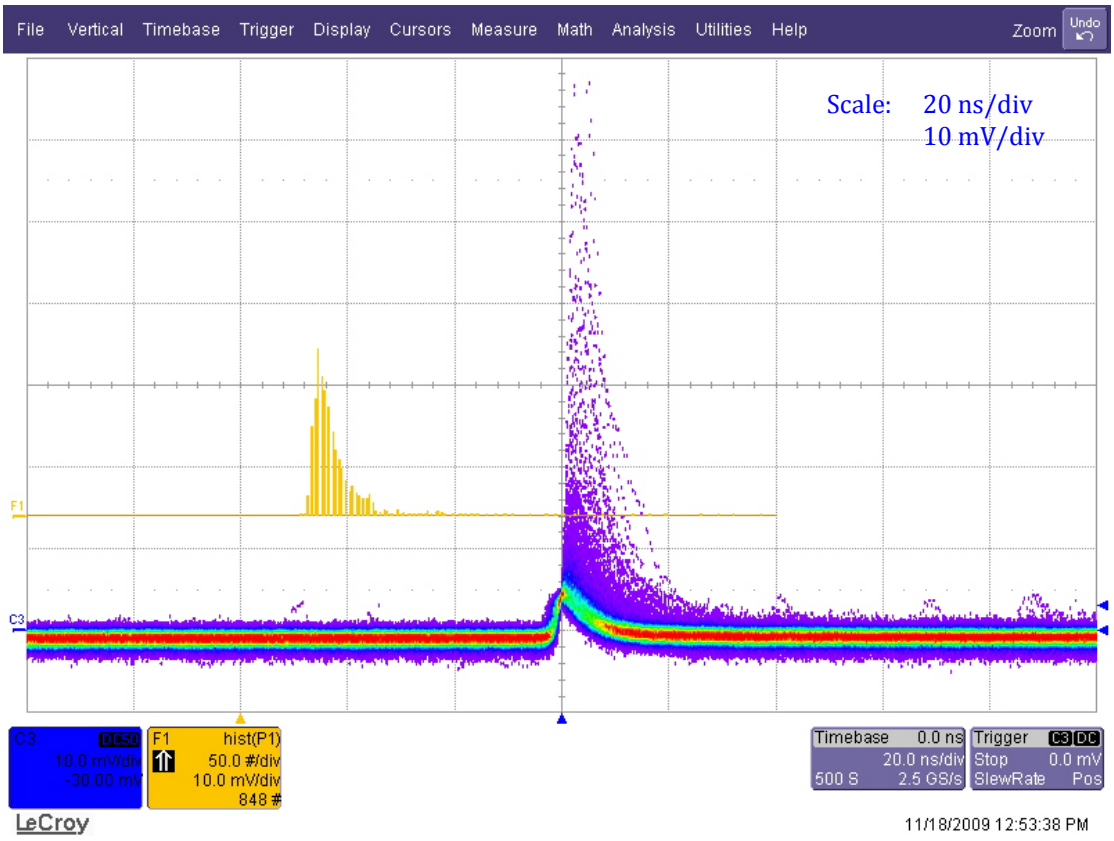

Figure 10: Persistence plot of multi-particle events and amplitude histogram (yellow).

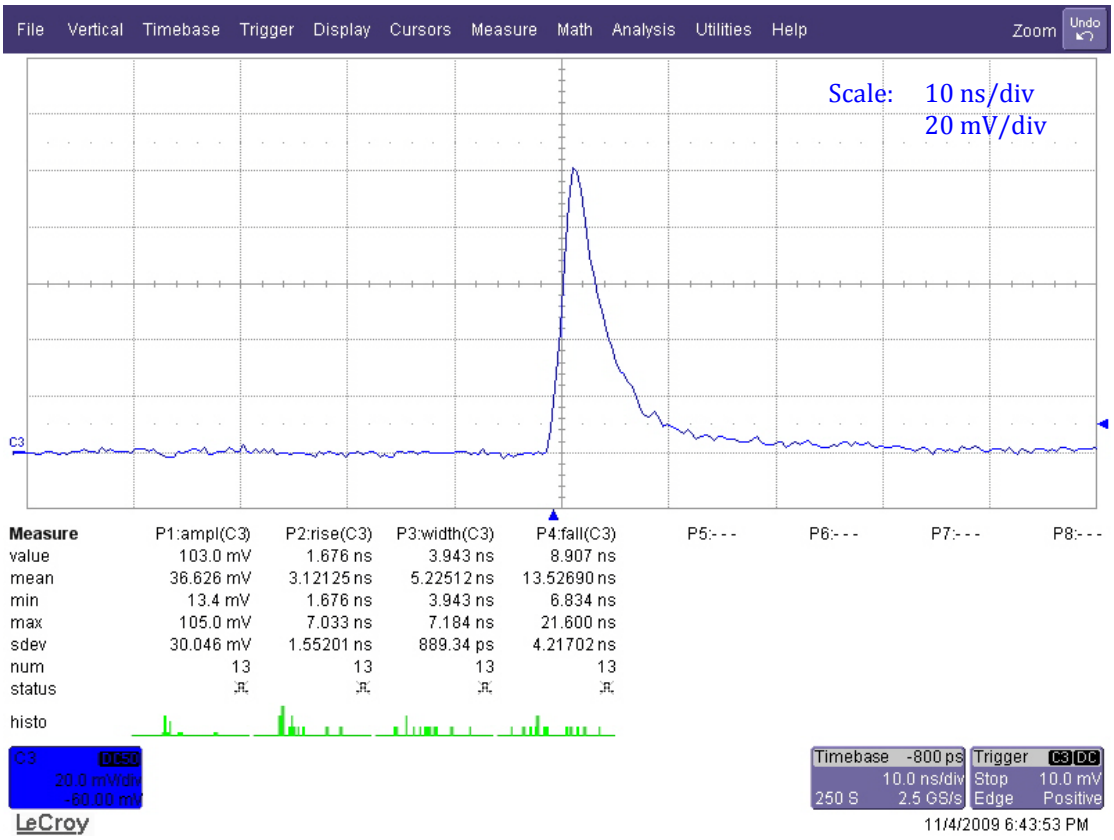

Figure 11: Multi-particle pulse of 28 MIPs.

5.3 Cascade mode

This applies to multi-particle bunches with time periods exceeding the response time of the detector. Such losses are likely caused after injection into the SPS and after the beam-energy ramp. Figure 12 shows a particle cascade lasting for 96 ns with an amplitude of 806 mV. This corresponds to a charge occupancy of about 4000 particles hitting the detector during the cascade. The peak detector current is 134 μA.

Figure 13 shows a persistence plot of multi-particle events in combination with particle cascades.

The quantitative limit of measurements is only given by the saturation of the preamplifier. Qualitatively, the detector recovers and is ready for next the measurement.

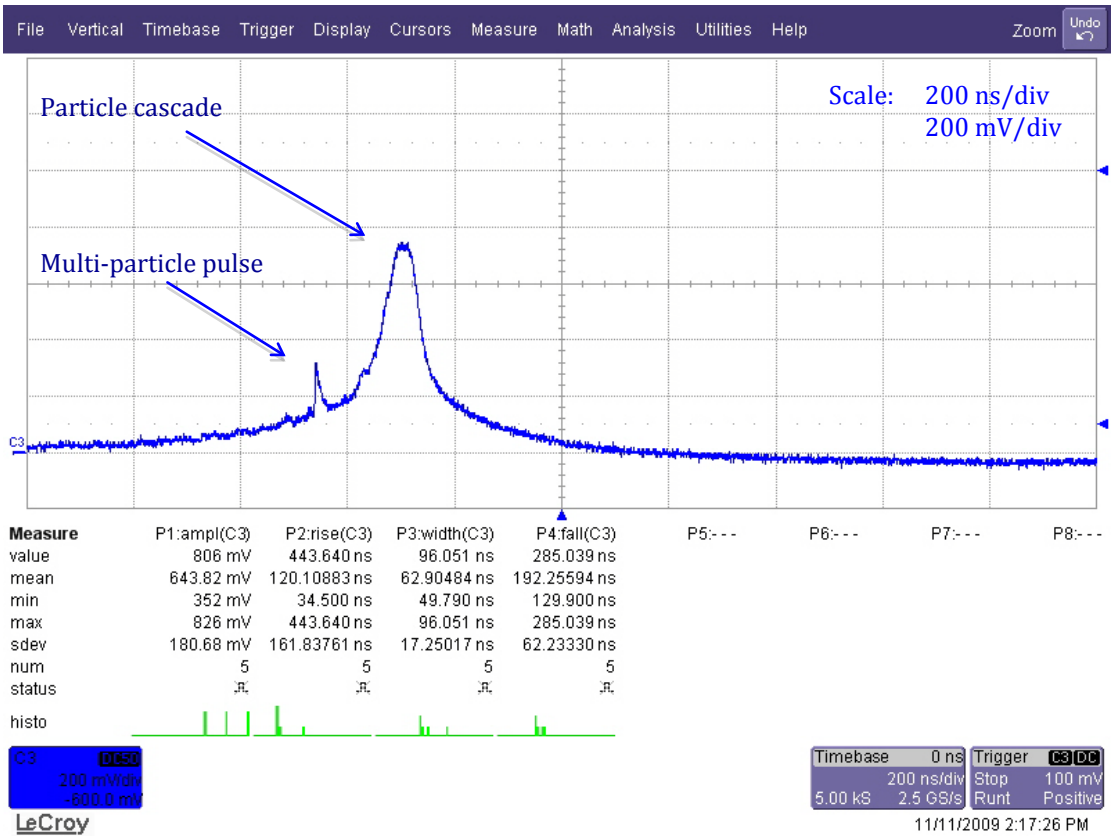

Figure 12: Particle cascade with a multi-particle pulse at the rising edge. About 4000 particles are hitting the detector in this example.

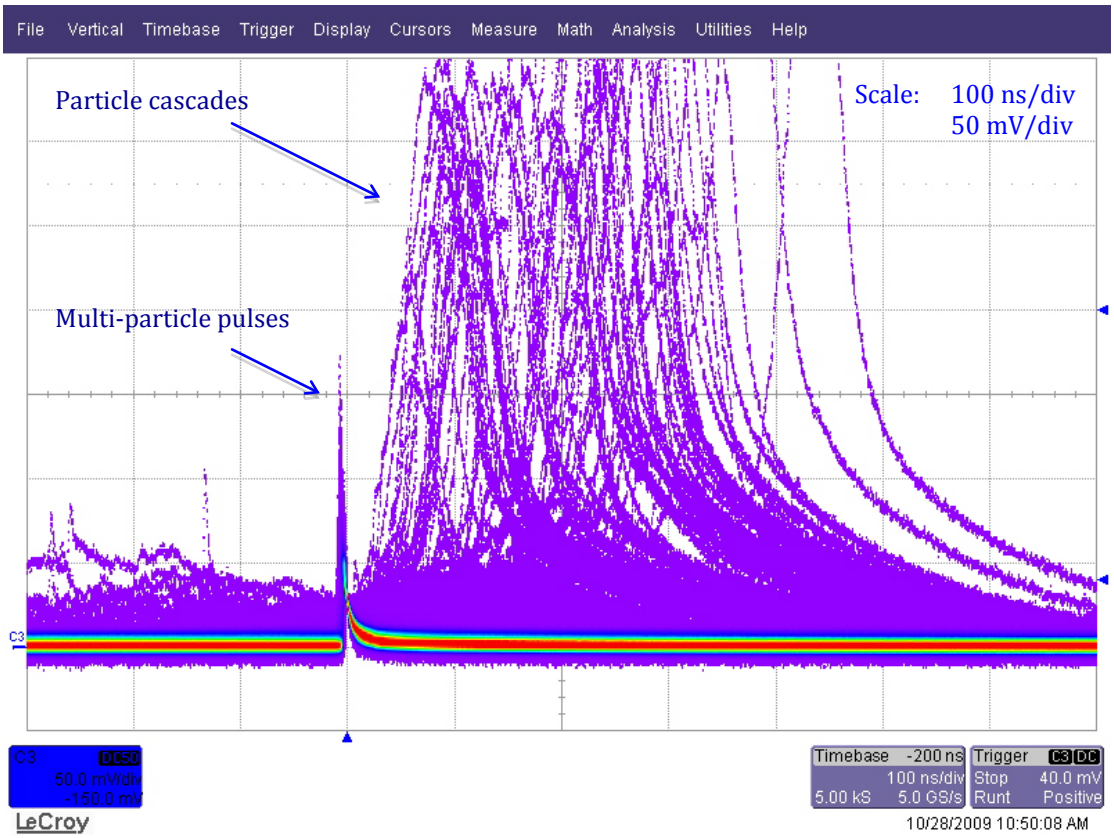

Figure 13: Multi-particle pulses and particle cascades.

5.4 High intensity mode

Figure 14 shows 10 µs long particle cascades in persistence mode with amplitudes up to 1 V, which is close to saturation of the detector electronics and corresponds to some 5×10^5 particles traversing the detector and a detector current of 167 µA. The recovery time of the electronics is of the order of 20 µs.

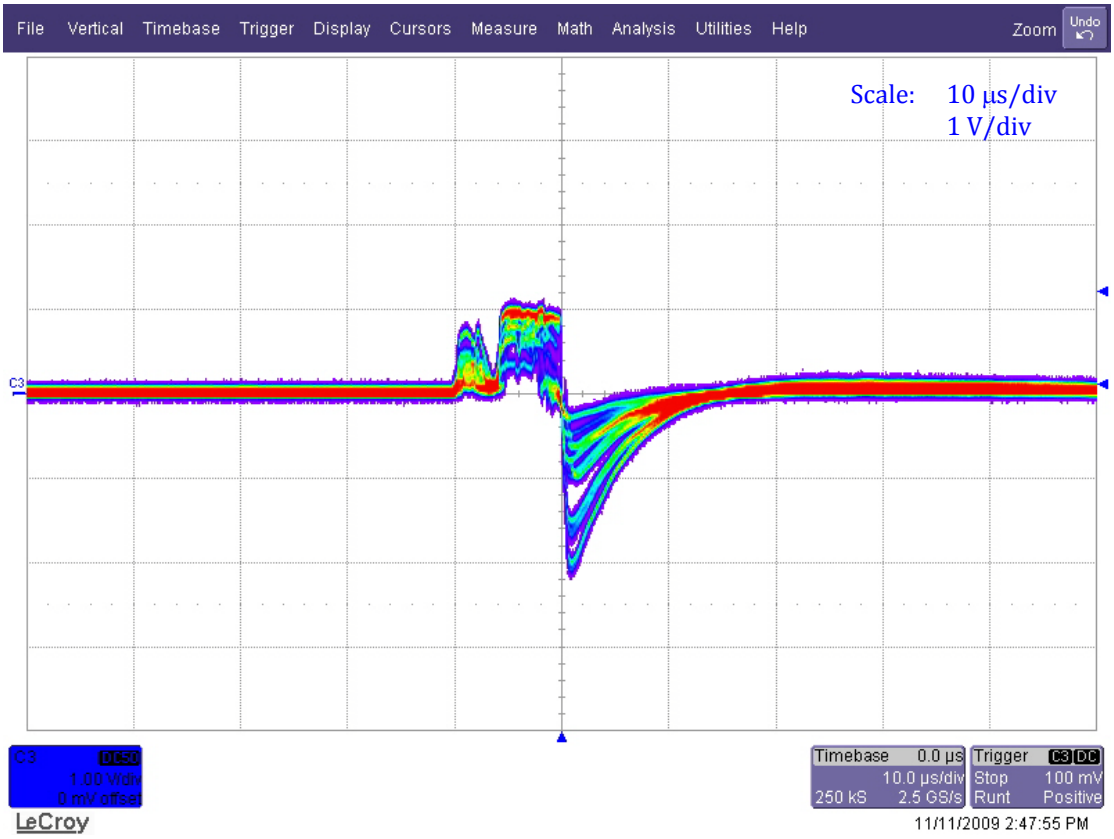

Figure 14: High intensity particle cascades where up to 5×10^5 particles traverse the detector. The negative undershoot indicates restoration of the preamplifier within 20 µs.

5.5 Background

There are two types of background signal:

- ➔ Electronic noise, coherent and incoherent,
- ➔ particle events, which are generated by the activated beam pipe.

Suppression of the electronic noise is described below, leading to an excellent overall noise behaviour.

5.5.1 Coherent electronic noise

a) Power converters
A 300 Hz coherent noise component was picked up from the magnet power converters (3rd order harmonic). This component was strong during physics beam, and weaker during coasting beam, LHC cycles and LHC operation. This noise component and its frequency spectrum are shown in Figure 15. The time response shows bursts with a maximum noise amplitude of 4 mV. The frequency spectrum shows the noise bandwidth of 50 kHz.

b) RF signal pick up
The detector has a very high bandwidth up to the GHz range. This is necessary for fast particle detection, but it implies a high sensitivity to RF-pickup from radio stations (100 MHz range), TV stations (400 MHz range) and GSM (1 and 1.6 GHz range). See Figure 16.

It was possible to limit coherent noise components with a 200 kHz high-pass filter and a 200 MHz low-pass filter at the input of the scope.

5.5.2 Incoherent electronic noise

Incoherent noise components come from the preamplifier and pick-up from the cable. Compensation was achieved by the 200 MHz bandwidth limitation of the scope.

5.5.3 Activation noise

Background noise from β-decays in the activated beam pipe was observed when the SPS beam was off (Figure 17). Some 2938 background events were recorded in 33 hours and 15 minutes, corresponding to 1.47 background events per minute, which makes activation noise unimportant in the present context.

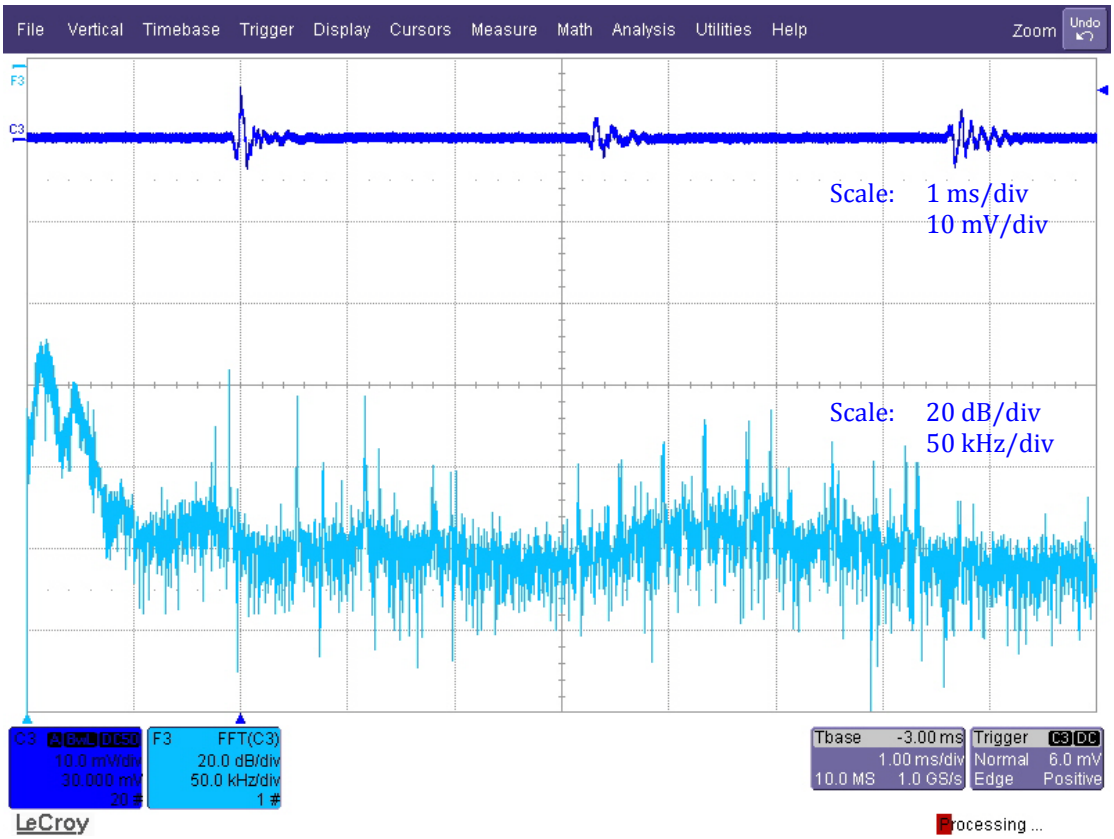

Figure 15: Coherent noise caused by 3rd order harmonics from power converters.

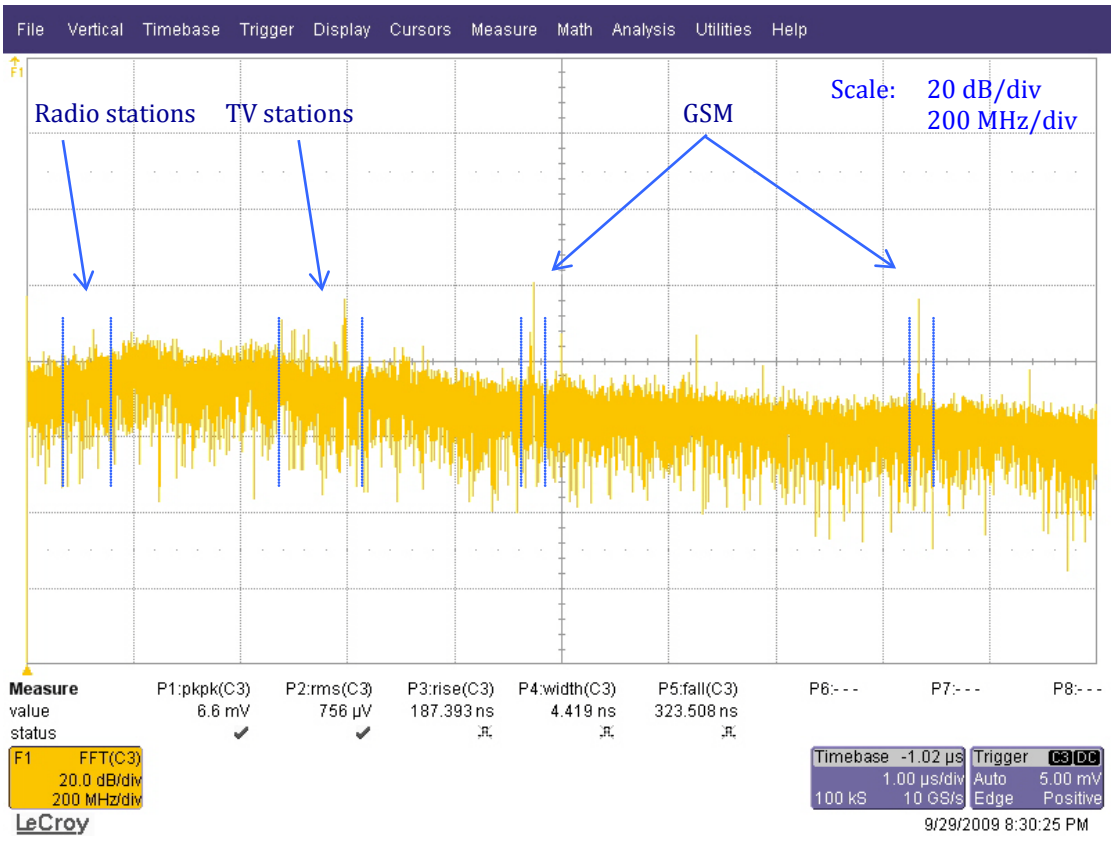

Figure 16: Frequency spectrum of RF noise.

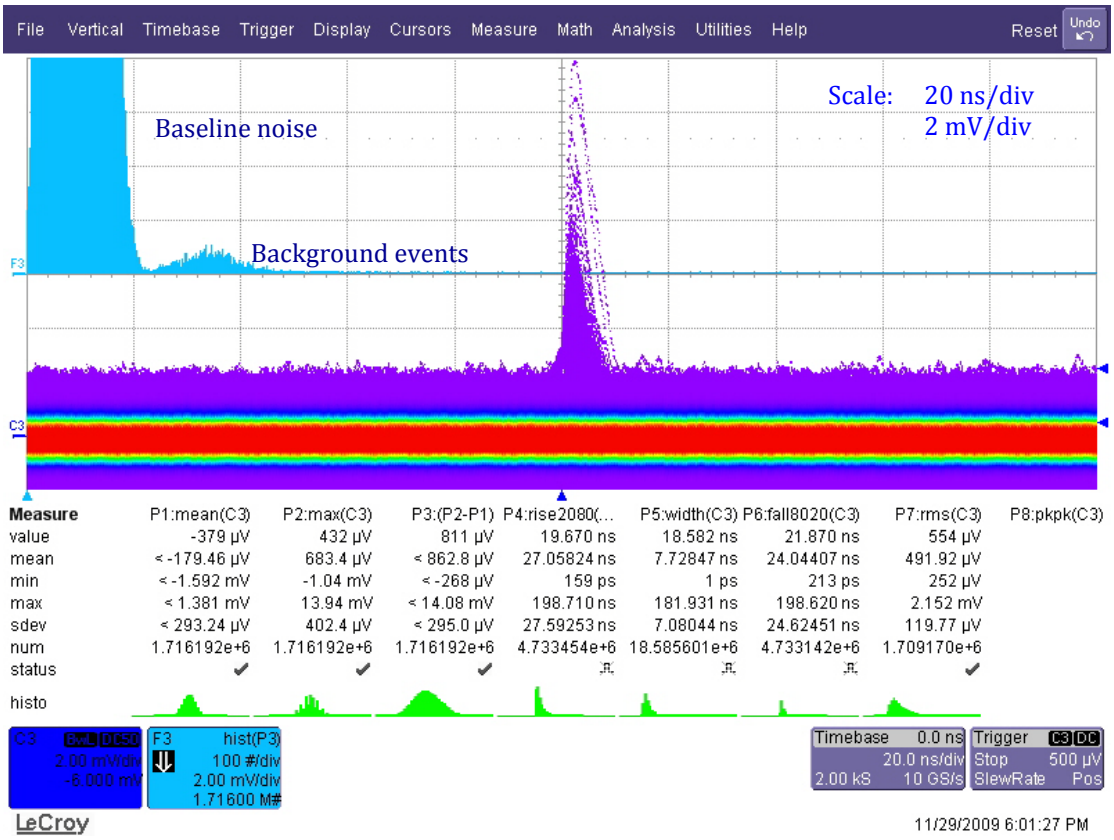

Figure 17: Background events from the activated beam pipe.

6 Example applications

6.1 Coasting beam halo measurements

During coasting beam operation (3.11.2009, MD on crystal extraction), the arrival time of lost particles with respect to the revolution frequency was recorded. Figure 18 shows the time traces of the revolution frequency (top: blue/red persistent mode, C2 trace) and the diamond signal (bottom: blue/red in persistent mode, C3 trace). The trigger threshold is set to 20 mV (see cursor at the right side of trace C3), which is unfortunately not clearly seen by the lower cut off of the amplitude distribution (middle: yellow, F1 trace). The arrival time distribution (top left: magenta, F2 trace) shows entries over a duration of about 7.8 µs reflecting the filling structure of the SPS with four PS batches. The equidistant spaced higher count rates match exactly the beginning of each PS batch with 72 bunches.

Figure 18: Beam losses measured during coasting-beam operation of the SPS.

6.2 Loss measurements with fixed SPS target beam

Figure 19 shows periodic losses at the RF-frequency of 200 MHz.

The signal amplitude exceeds 120 mV, and the pulse width is of the order of 90 ns, which corresponds to an incident number of particles of some 500, and to a detector current of 20 μA.

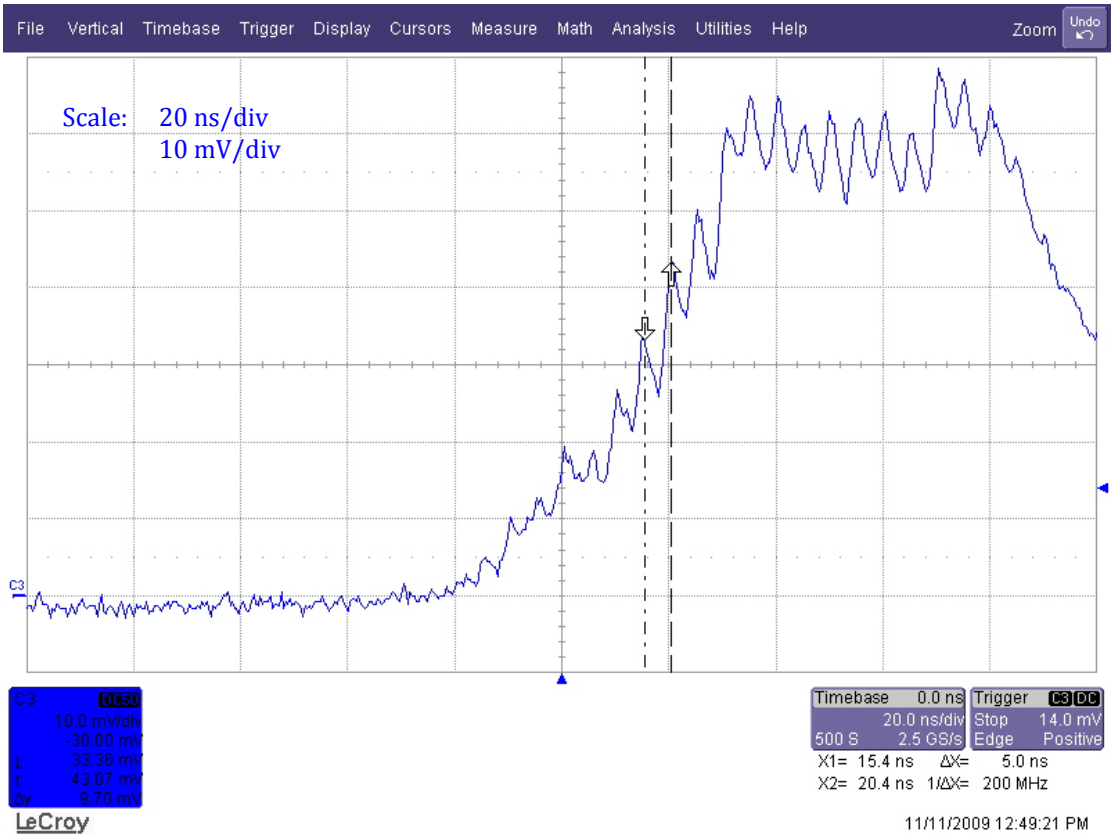

Figure 19: Particle-loss cascade at the 200 MHz RF frequency of the SPS.

The 5 ns timing RF structure of the SPS can clearly be observed and demonstrates the excellent double-pulse resolution of the detector.

7 Summary

A pCVD diamond detector was tested downstream of a collimator in the SPS BA5 during the beam set-up for LHC. A 250 m long CK50 cable connected the detector to the instrumentation in the counting room.

Single-particle detection is covered by the detector as well as multi-particle events and particle cascades up to the resolution limit set by the saturation of the electronics at 350 simultaneously impinging MIP particles.

The intrinsic double-pulse resolution of the CVD diamond detector is less than 1 ns. Due to the length of the signal cable and the capacitance of the detector stack, the double-pulse resolution is degraded to 5 ns in this application. Nevertheless, the high temporal resolution and the fast recovery time make it possible to detect the arrival of particles between the nominal bunch positions.

8 Acknowledgments

We acknowledge the help of Ian McGill from CERN PH/DT, Rui De Oliveira from CERN EN/ICE and Claudine Chery from CERN BE/BI for a proper detector assembly and Phil Bryant ex CERN for proof-reading the article.

9 References

[1] H. Frais-Kölbl, E. Griesmayer, H. Pernegger, H. Kagan, *A Fast Low-Noise Charged Particle CVD Diamond Detector*, IEEE Trans. on Nuclear Science, Vol. 51, No. 6, p. 3833 – 3837, December 2004.

[2] CERN RD-42 Collaboration, *Radiation hard diamond sensors for future tracking applications*, NIM A 565 (2006) 278–283.

[3] CERN RD-42 Collaboration, *CVD Diamond Radiation Detector Development* (http://rd42.web.cern.ch/RD42/).

[4] V. Cindro et. al, *The ATLAS Beam Conditions Monitor*, JINST, February 2008.

* * *